Techniques to sort Bessel beams

Angela Dudley[a], Thandeka Mhlanga[a,b], André McDonald[a], Filippus S. Roux[a], Martin Lavery[c], Miles Padgett[c], and Andrew Forbes*[a,b,d]
[a] CSIR National Laser Centre, PO Box 395, Pretoria 0001, South Africa;
[b] Stellenbosch University, Private Bag X1, Matieland 7602, South Africa;
[c] Department of Physics and Astronomy, University of Glasgow, Glasgow, UK;
[d] School of Physics, University of KwaZulu-Natal, Private Bag X54001, Durban 4000, South Africa

ABSTRACT

In this work we will present two techniques for the measurement of superimposed higher-order Bessel beams. In the first technique we will outline a simple approach using only a spatial light modulator and a Fourier transforming lens to decompose the OAM spectrum of an optical field. We test this approach on symmetric and non-symmetric superpositions of non-diffracting higher-order Bessel beams. Our second procedure consists of two refractive optical elements which perform a Cartesian to log-polar coordinate transformation, translating helically phased beams into a transverse phase gradient. By introducing two cylindrical lenses we can focus each of the azimuthal modes associated with each Bessel beam to a different lateral position in the Fourier plane, while separating the radial wave-vectors in the image-plane.

Keywords: Sorting orbital angular momentum, modal decomposition, Bessel beams

1. INTRODUCTION

Numerous publications have been dedicated to optical fields which carry orbital angular momentum (OAM), ranging from Laguerre-Gaussian [1], Bessel-Gauss [2] and Airy beams [3]. Each of these fields has an azimuthal angular dependence of $\exp(il\theta)$ [1, 4-6] where l is the azimuthal index and θ is the azimuthal angle. The fact that these fields offer an unbounded state space has made them advantageous for increasing the amount of information that can be encoded onto a single-photon [7-11].

In this work we are interested in higher-order Bessel beams as an OAM-carrier as these fields offer other useful properties such as their ability to propagate diffraction-free over a finite distance [12-21] and reconstruct after encountering an obstacle [22]. Exploiting these properties of Bessel beams will make them very useful in the field of long-range, broad bandwidth communication systems. However, in order for these fields to be a success in the area of optical communication, efficient techniques for extracting the information they carry (i.e. their azimuthal mode indices) need to exist.

The 'fork' diffraction grating can be used to couple light of a particular OAM state into a single-mode fibre [6], but this requires that one must test for all possible states simultaneously. Attempts to develop more complicated holograms which test multiple states have been made [9, 23], however their efficiency is inversely proportional to the number of states being sampled. An alternative setup that does not alter the OAM state during the measurement procedure is a Mach-Zehnder interferometer with two Dove prisms in each arm [24, 25], which sorts odd and even OAM states into two separate ports. Recently it has been demonstrated that two spatial light modulators (or refractive optical elements) in conjunction with a lens can be used to convert the OAM state of light to a specified lateral position [26, 27].

*aforbes1@csir.co.za

Laser Beam Shaping XIV, edited by Andrew Forbes, Todd E. Lizotte, Proc. of SPIE Vol. 8843, 884306

In this manuscript we make use of two techniques to measure the OAM spectrum of higher-order Bessel beams. The first technique involves a spatial light modulator and a Fourier transforming lens to decompose the OAM spectrum of an optical field [28-30]. We implement this technique on symmetric and non-symmetric superpositions of non-diffracting higher-order Bessel beams. The second technique makes use of the above mentioned refractive optical elements to extract the information encoded in higher-order Bessel beams [31, 32]. We first show that we can resolve forty-one OAM states and forty-one radial components of our higher-order Bessel beams separately. By introducing cylindrical lenses into the optical setup, we illustrate that one is able to extract both the OAM states and radial components of the modes simultaneously. In this configuration we resolve twenty-one OAM states with fairly low cross-talk levels.

2. THEORY

Modal decomposition

Since the angular harmonics, $\exp(il\varphi)$, are orthogonal over the azimuthal plane, the OAM-carrying fields and their superpositions may be expressed in terms of such harmonics as follows

$$u(r,\phi,z)=\frac{1}{\sqrt{2\pi}}\sum_{l}a_l(r,z)\exp(il\phi), \tag{1}$$

with

$$a_l(r,z)=\frac{1}{\sqrt{2\pi}}\int_0^{2\pi}u(r,\phi,z)\exp(-il\phi)d\phi. \tag{2}$$

The relative weighting of the power contained in each azimuthal mode can then be defined as [3]:

$$P_l(z)=\frac{\int_0^{\infty}\left|a_l(r,z)\right|^2 rdr}{\sum_l\int_0^{\infty}\left|a_l(r,z)\right|^2 rdr}. \tag{3}$$

Refractive optics

The technique used for the measurement of the OAM spectrum and the radial components of Bessel beams, consists of two refractive optical elements [26, 27, 33, 34] which map a position in an input plane (x,y) to a position in the output plane (u,v) by a conformal mapping [35-37]

$$u=-a\ln\left(\frac{\sqrt{x^2+y^2}}{b}\right)=-a\ln\left(\frac{R}{b}\right), \tag{4}$$

and

$$v=a\arctan\left(\frac{y}{x}\right). \tag{5}$$

Equation 4 illustrates that the vertical coordinate varies as a function of the radial component, R. The first refractive element which performs the log-polar mapping as given in Eqs (4) and (5), has a phase profile given by

$$\phi_1(x,y)=\frac{a}{f(n-1)}\left[y\arctan\left(\frac{y}{x}\right)-x\ln\left(\frac{\sqrt{x^2+y^2}}{b}\right)+x-\frac{1}{a}\underbrace{\left(\frac{1}{2}(x^2+y^2)\right)}_{lens\ \ term}\right]. \tag{6}$$

f is the focal length of the lens integrated in the refractive optical element and n its refractive index. The parameter a controls the width of the azimuthal projection on the second refractive optical element, where $a = d/2\pi$ and d is the length of the second refractive optical element along the y-axis; b controls the scaling of the radial component and may

be chosen independently of a. The second refractive optical element is placed at a distance of f behind the first and corrects any unwanted phase distortions associated with the first refractive optical element. It has a phase profile of

$$\phi_2(x,y) = -\frac{ab}{f(n-1)}\left[\exp\left(-\frac{u}{a}\right)\cos\left(\frac{v}{a}\right) - \frac{1}{ab}\underbrace{\left(\frac{1}{2}(x^2+y^2)\right)}_{lens\ \ term}\right]. \tag{7}$$

A schematic of the concept, where the above mentioned refractive optical elements are used to resolve both the azimuthal and radial components, is given in Fig. 1.

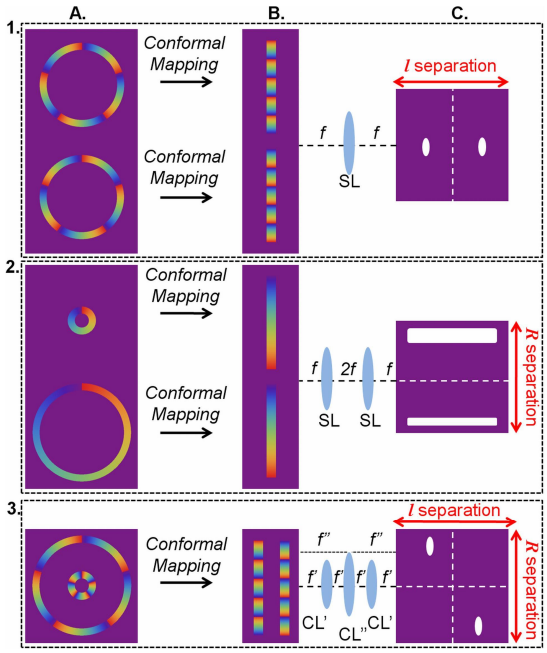

Fig. 1. Case 1, column A: Annular rings (Fourier transform of Bessel beams) of the same radius but different azimuthal components (l = -5 and l = +5) are mapped to transverse momentum modes represented by the linear phase variations in column B. A spherical lens (SL) arranged in a 2-f configuration maps the transverse momentum modes to unique x-coordinates in column C. Case 2, column A: Annular rings of the same azimuthal components (l = +1) but different radii are mapped to transverse momentum modes represented by the linear phase variations in column B. Spherical lenses (SL) arranged in a 4-f configuration image the transverse momentum modes to unique y-coordinates in column C. Case 3, column A: Superimposed annular rings of different radii and different azimuthal components (l = -5 and l = +5) are mapped to transverse momentum modes represented by the linear phase variations in column B. Cylindrical lenses (CL) arranged in a 4-f configuration map the transverse momentum modes to unique x- and y-coordinates in column C, respectively.

The conformal mapping that is described by Eqs (4) and (5) and achieved by the phase profile given in Eq. (6) is depicted to occur between columns A and B in Fig. 1. The annular ring structure (Fourier transform of Bessel beams) possessing a particular azimuthal phase variation of a particular radial component is mapped to a linear phase variation. Each of the cases represented in Fig. 1 resembles the concept for separating azimuthal components (case 1), radial components (case 2) and both azimuthal and radial components simultaneously (case 3). In case 1, two annular rings possessing the same radial components, but different azimuthal orders (l = -5 and l = +5), given in column A, are transformed to a linear phase variation as represented in column B. A spherical lens is placed after the second refractive optical element to focus the transformed beam to a specified spot in the focal plane, represented in column C. The position of the spot varies along the x-direction as a function of the incident azimuthal order and is defined by

$$t_l = \frac{\lambda f}{d} l. \tag{8}$$

Case 2 represents the concept for resolving the radial component of the incident beam. Two annular rings possessing the same azimuthal component (l = +1), but different radial components as given in column A, are transformed to a linear phase variation represented in column B. By arranging two spherical lenses in a 4-*f* configuration, the unravelled linear phase variation is imaged to the plane represented in column C and varies along the *y*-direction as a function of the incident radial component as defined by Eq. (3). To combine both of the techniques represented in cases 1 and 2, to simultaneously resolve the azimuthal and radial components to *x*- and *y*-coordinates respectively, cylindrical lenses are arranged in a 4-*f* configuration, as depicted in case 3. The *x*-axis at the plane contained in column B is Fourier transformed to a specified *x*-position at column C (achieved by cylindrical lens CL''), while cylindrical lenses CL' image the *y*-axis at column B's plane to that in column C. This results in the transverse momentum modes at column B being transformed to a specified position on the *x*-axis at column C, while simultaneously imaging the unravelled annular ring to a specified position on the *y*-axis. The example given in case 3 consists of a superposition of two annular rings that are resolved to two different spots, whose *x*- and *y*-coordinates are related to their azimuthal and radial components respectively.

3. EXPERIMENTAL METHODOLOGY

Modal decomposition

The experimental realization of the modal decomposition technique comprises of two parts: the generation and then decomposition of the field, and is shown schematically in Fig. 2(a). A Gaussian beam (Fig. 2(b)) was expanded through a 5× telescope and directed onto the liquid crystal display of SLM_1 which was programmed to produce various superposition fields of OAM carrying Bessel beams. The Bessel fields were then magnified with a 10× objective and directed to the second SLM (SLM_2) for executing the modal decomposition. This was accomplished by executing an inner product of the incoming field with the match filter set to $\exp(il\varphi)$, for various l values, and for particular radial (r) positions on the field. The Fourier plane is shown in Fig. 2(f) where we require only the intensity at the origin of this plane.

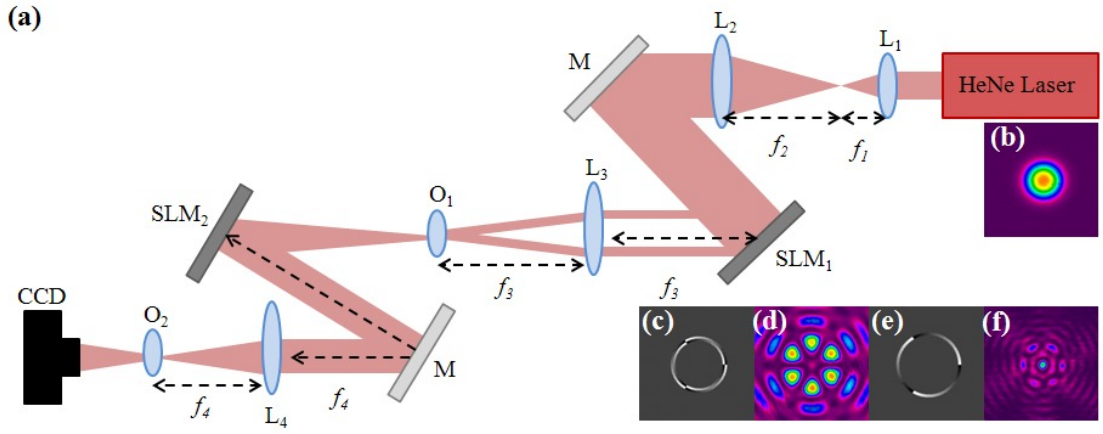

Fig. 2. (a) A schematic of the experimental setup for performing the modal decomposition. L: Lens (f_1 = 15 mm; f_2 = 75 mm; f_3 = 200 mm and f_4 = 200 mm); M: Mirror; SLM: Spatial light Modulator; O: Objective; CCD: CCD Camera. The objective, O_2, was placed at the focus (or Fourier plane) of lens, L_4. (b) The Gaussian beam used to illuminate SLM_1. (c) The digital hologram used to generate the optical field of interest (d) and the digital hologram (e) used to extract the weightings of the modes from the inner product (f).

Refractive optics

The experimental setup is presented in Fig. 3 (a). A HeNe laser was expanded through a telescope (lenses L1 and L2) to illuminate the liquid crystal display of a SLM. The SLM was programmed to produce the Fourier transform of Bessel beams of various azimuthal and radial orders which were imaged onto the entrance of the mode sorter, located at the first refractive optical element (R1). To produce the Fourier transform of a Bessel beam, an annular ring containing a

particular azimuthal order was encoded onto the SLM; such an example is given in Fig. 3 (b). Alternating sets of pixels surrounding the annular ring were assigned phase values of 0 and π, producing an amplitude transmission of 0 on our phase-only SLM [38]. The resulting annular rings were propagated through the mode sorter (denoted by refractive optical elements, R1 and R2), where R1 performed a log-polar mapping thus transforming the azimuthal modes to transverse momentum modes, while consequently mapping the radial component to a unique latitude. The second refractive optical element (R2) corrected the unwanted phase associated with R1. The phase profiles of the refractive optical elements R1 and R2, obtained from Eqs (6) and (7), are presented in Figs 3 (c) and 3 (d) respectively.

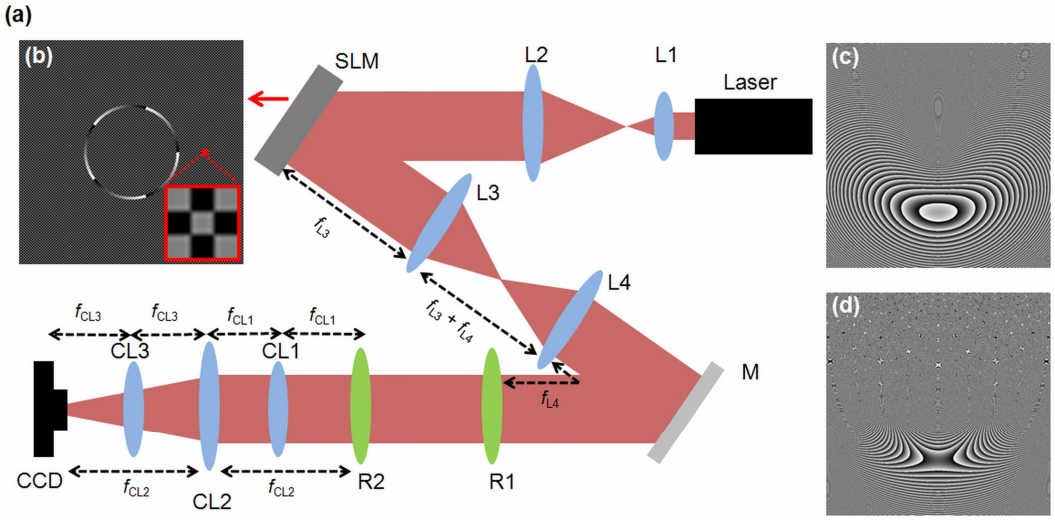

Fig. 3. (a) Schematic of the experimental setup for efficiently sorting the azimuthal and radial components of Bessel beams. L, lens (f_{L1} = 15 mm, f_{L2} = 125 mm, f_{L3} = 500 mm, f_{L4} = 500 mm); SLM, spatial light modulator; M, mirror; R, refractive optical element; CL, cylindrical lens (f_{CL1} = 50 mm (orientated to focus the *y*-axis), f_{CL2} = 100 mm (orientated to focus the *x*-axis), f_{CL3} = 50 mm (orientated to focus the *y*-axis)); CCD, CCD camera. (b) The phase profile encoded on the SLM and a zoomed-in insert of the alternating phase values surrounding the ring-slit. (c) and (d) The phase profiles of the refractive optical elements R1 and R2, respectively.

4. RESULTS AND DISCUSSION

Modal decomposition

For the modal decomposition technique the Bessel field was divided radially into 10 sections, with each section sequentially apertured by an annular ring (as illustrated in Fig. 4). The azimuthal phase within the annular ring was varied from –4 to +4 in the *l* index. Thus the decomposition of the field of interest was executed as a function of radial co-ordinate and azimuthal mode. This allows for the OAM spectrum, $a_l(r,z)$ to be found at any radial position across the beam.

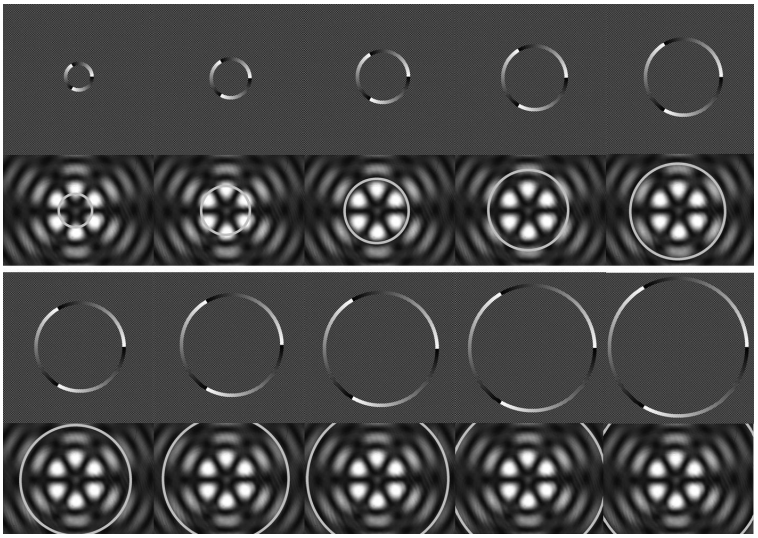

Fig. 4. The field of interest was divided radially, and an annular ring was programmed onto the second SLM in order to execute the inner product at only this radius. The phase within the annular ring was varied in the azimuthal angle for various values of l.

The experimentally measured weighting coefficients for a superposition of two Bessel beams (with azimuthal indices l = +3 and -3) is given in Fig. 5 it is evident that although the global OAM of this particular field is zero, the local OAM varies radially across the field for azimuthal indices of +3 and -3.

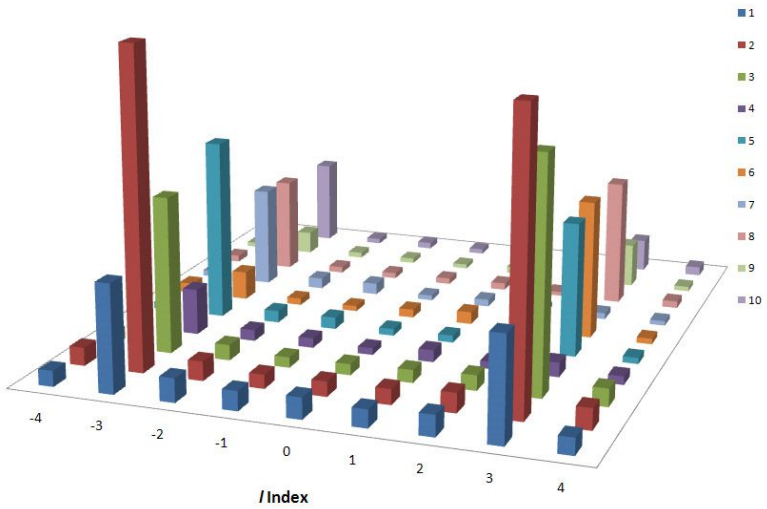

Fig. 5. The measured OAM spectrum (for l values of –4 to +4) as a function of the radial position. The height of each bar represents the measured coefficients $|a_l|^2$.

Refractive optics

Annular rings of radius, R = 1320 μm, having azimuthal orders ranging from l = -10 to +10 were generated and directed through the mode sorter. An example of a hologram, for an azimuthal order of l = -5, encoded on the SLM and the annular ring produced at the plane of R1 together with its Fourier transform are given in the first row of Fig. 6 ((a) – (c), respectively). The unravelled transverse momentum mode at the plane of R2 was focused by a cylindrical lens having a focal length of f = 100 mm, producing an elongated lateral spot shown in Fig.6 (d), with its theoretical prediction given alongside in Fig. 6 (e). We illustrate that the result can be improved by replacing the three cylindrical lenses with a single spherical lens (f = 250 mm), producing the experimentally recorded lateral spot in Fig. 6 (f) which is in very good

agreement with its theoretical prediction in Fig. 6 (g). The white dotted line represents the position for the lateral spot for an azimuthal mode of $l = 0$. Apertures in the detector plane were centred on the expected spot positions and the intensity in each of the apertures was measured for each input mode. The relative fraction of the OAM state was determined and is presented in Fig. 6 (h).

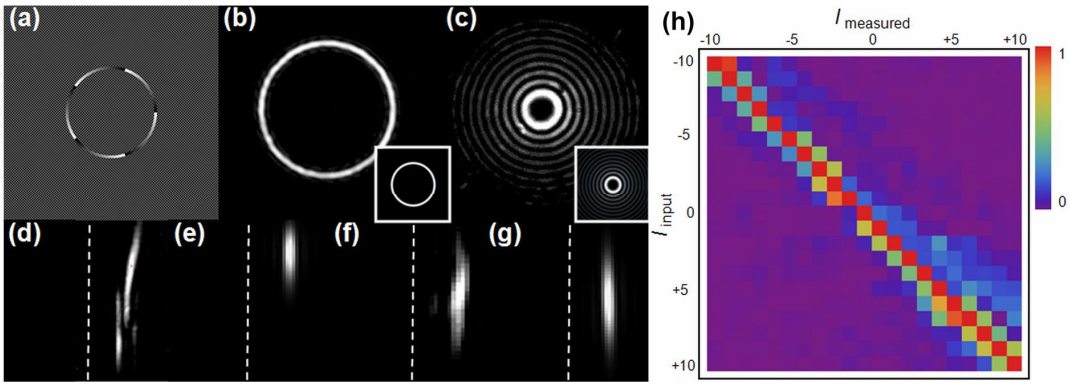

Fig. 6. (a) The hologram, (b) annular ring, and (c) Bessel beam for a radial component of $R = 1320$ μm and an azimuthal component of $l = -5$. The theoretical results are given as inserts. (d) The experimentally recorded and (e) theoretically calculated lateral spot when cylindrical lenses are used (as in case 3 of Fig. 1). (f) The experimentally recorded and (g) theoretically calculated lateral spot when a spherical lens ($f = 250$ mm) is used. (h) Relative fractions of the intensity at each detector position for incoming OAM states ranging from $l = -10$ to $+10$ (for $R = 1320$ μm).

The radial component of the annular ring entering the mode sorter was varied from values of $R = 920$ to 2520 μm. An example of a hologram and its corresponding annular ring and Fourier transform is given in the first row of Fig. 7 ((a) – (c)). The transformed unravelled annular rings, at the plane of R2, were imaged onto the CCD, with the use of cylindrical lenses CL1 and CL3 and an example is depicted in Fig. 7 (d), together with its theoretical prediction in Fig. 7 (e). We illustrate that the result can be improved by replacing the three cylindrical lenses with two spherical lenses ($f = 250$ mm), as in case 2 of Fig. 1, imaging the unravelled transverse momentum mode to the CCD as in Fig. 7 (f) which is in very good agreement with its theoretical prediction in Fig. 7 (g). The white dotted line marks a common reference on the CCD image. Similarly in detecting the radial components, apertures in the detector plane are centred on the expected line positions and relative fractions of the radial spectrum for various input modes are determined and presented in Fig. 7 (h).

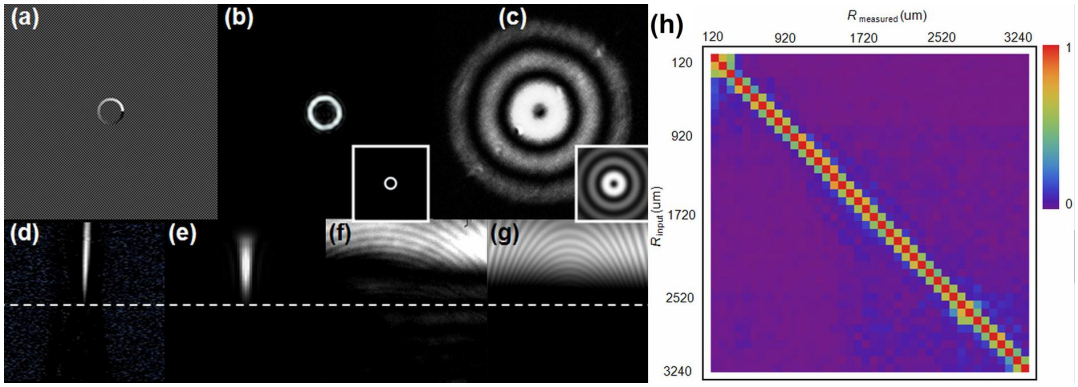

Fig. 7. (a) The hologram, (b) annular ring, and (c) Bessel beam for a radial component of $R = 360$ μm and an azimuthal component of $l = +1$. The theoretical results are given as inserts. (d) The experimentally recorded and (e) theoretically calculated lateral spot when cylindrical lenses are used (as in case 3 of Fig. 1). (f) The experimentally recorded and (g) theoretically calculated unravelled transverse momentum mode when two spherical lenses ($f = 250$ mm) are used. (h) (b) Relative fractions of the intensity at each detector position for incoming radial components ranging from $R = 120$ to 3220 μm (for $l = +1$).

Multiple annular rings were also directed through the mode sorter and an example is presented in Fig 8. An example of a hologram containing two annular rings of differing radii and azimuthal modes is given in Fig. 8 (a) together with its

corresponding annular ring field and Fourier transform (superimposed Bessel beams) in Figs 8 (b) and (c), respectively. The separation of the two azimuthal and two radial components, when using cylindrical lenses CL1, CL2 and CL3, is depicted in Fig. 8 (d) accompanied with the theoretical prediction in Fig. 8 (e), illustrating that the mode sorter is capable of distinguishing superimposed azimuthal modes. There is fairly good agreement in terms of the locations of the experimentally recorded lateral spots (Fig. 8 (d)) and their theoretical predictions (Fig. 8 (e)).

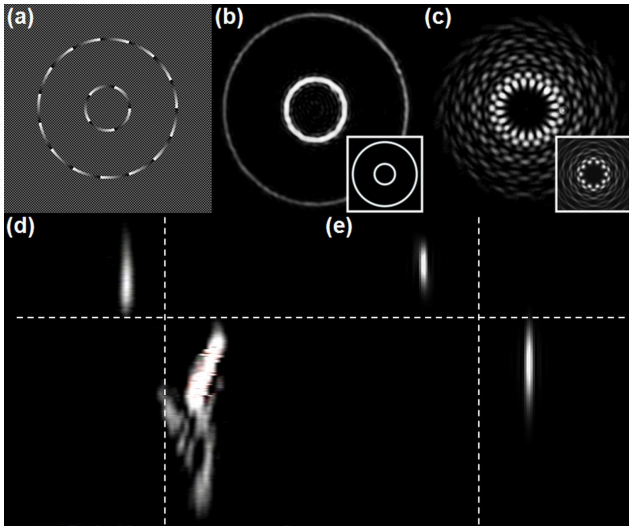

Fig. 8. (a) Digital hologram of multiple azimuthal and radial orders R_1 = 680 μm, R_2 = 2120 μm, l_1 = -5, l_2 = +15, and (b) the corresponding annular ring field and (c) Fourier transform (superimposed Bessel beams). The theoretical results are given as inserts. (d) The corresponding experimental and (e) theoretical spots produced at the plane of the CCD.

5. CONCLUSION

We have demonstrated a modal decomposition technique for the extraction of the OAM spectrum of an optical field which requires only an SLM and a lens [28-30]. For a superposition of two Bessel beams of azimuthal indices l = +3 and -3, we find that while the global OAM is zero, the local OAM spectrum changes radially across the beam. For the refractive optic case, we have illustrated the separation of higher-order Bessel beams in both their azimuthal and radial bases [31, 32]. The ability to extract encoded information across two higher-dimensional state spaces will prove very useful in quantum communication and information systems. Although there is a slight overlap between neighbouring modes in separating both the OAM and radial modes (and even more so in the case of implementing cylindrical lenses), we suggest first separating the OAM modes into odd and even ports [24, 25] to decrease any cross-talk.

REFERENCES

[1] Beijersbergen, M. W., Allen, L., Van der Veen, H. E. L. O., and Woerdman, J. P., "Astigmatic laser mode converters and the transferof orbital angular momentum," Opt. Commun. **96**, 123–132 (1993).

[2] Arlt, J., and Dholakia, K., "Generation of high-order Bessel beams by use of an axicon," Opt. Commun. **177**, 297–301 (2000).

[3] Sztul, H. I., and Alfano, R. R., "The Poynting vector and angular momentum of Airy beams," Opt. Express **16**, 9411–9416 (2008).

[4] Allen, L., Beijersbergen, M. W., Spreeuw, R. J. C., and Woerdman, J. P.,"Orbital angular momentum of light and the transformation of Laguerre–Gaussian laser modes," Phys. Rev. A **45**, 8185–8189 (1992).

[5] He, H., Friese, M. E. J., Heckenberg, N. R., and Rubinsztein-Dunlop, H., "Direct observation of transfer of angular momentum to absorptive particles from a laser beam with a phase singularity,"Phys. Rev. Lett. **75**, 826–829 (1995).

[6] Mair, A., Vaziri, A., Weihs, G., and Zeilinger, A., "Entanglement of the orbital angular momentum states of photons," Nature **412**, 313–316 (2001).

[7] Molina-Terriza, G., Torres, J. P., and Torner, L., "Twisted photons," Phys. Rev. Lett. **88**, 013601 (2001).

[8] Vaziri, A., Weihs, G., and Zeilinger, A., "Experimental two-photon, three-dimensional entanglement for quantum communication," Phys. Rev. Lett. **89**, 240401 (2002).
[9] Gibson, G., Courtial, J., Padgett, M., Vasnetsov, M., Pas'ko, V., Barnett, S., and Franke-Arnold, S., "Free-space information transfer using light beams carrying orbital angular momentum," Opt. Express **12**, 5448–5456 (2004).
[10] Barreiro, J. T., Wei, T. C., and Kwiat, P. G., "Beating the channel capacity limit for linear photonic superdense coding," Nat. Phys. **4**, 282 (2008).
[11] Leach, J., Jack, B., Romero, J., Jha, A. K.,Yao, A. M., Franke-Arnold, S., Ireland, D. G., Boyd, R. W., Barnett, S. M, Padgett, M. J., "Quantum correlations in optical angle-orbital angular momentum variables," Science **329**, 662–655 (2010).
[12] Durnin, J., Miceli, J. J., and Eberly, J. H., "Diffraction-free beams," Phys. Rev. Lett. **58**(15), 1499–1501 (1987).
[13] R. M. Herman, and T. A. Wiggins, "Production and uses of diffractionless beams," J. Opt. Soc. Am. A **8**(6), 932–942 (1991).
[14] Arlt, J., and Dholakia, K, "Generation of high-order Bessel beams by use of an axicon," Opt. Commun. **177**(1-6), 297–301 (2000).
[15] Turunen, J., Vasara, A., and Friberg, A. T., "Holographic generation of diffraction-free beams," Appl. Opt. **27**(19), 3959–3962 (1988).
[16] Vasara, A., Turunen, J., and Friberg, A. T., "Realization of general nondiffracting beams with computer-generated holograms," J. Opt. Soc. Am. A **6**(11), 1748–1754 (1989).
[17] Lee, H. S., Stewart, B. W., Choi, K., and Fenichel, H., "Holographic nondiverging hollow beam," Phys. Rev. A **49**(6), 4922–4927 (1994).
[18] Indebetouw, G., "Nondiffracting optical fields: some remarks on their analysis and synthesis," J. Opt. Soc. Am. A **6**(1), 150–152 (1989).
[19] Davis, J. A., Carcole, E., and Cottrell, D. M., "Nondiffracting interference patterns generated with programmable spatial light modulators," Appl. Opt. **35**(4), 599–602 (1996).
[20] Davis, J. A., Carcole, E., and Cottrell, D. M., "Intensity and phase measurements of nondiffracting beams generated with a magneto-optic spatial light modulator," Appl. Opt. **35**(4), 593–598 (1996).
[21] Paterson, C., and Smith, R., "Higher-order Bessel waves produced by axicon-type computer-generated holograms," Opt. Commun. **124**(1-2), 121–130 (1996).
[22] Bouchal, Z., Wagner, J., and Chlup, M., "Self-reconstruction of a distorted nondiffracting beam," Opt. Commun. **151**, 207 – 211 (1998).
[23] Khonina, S. N., Kotlyar, V. V., Skidanov, R. V., Soifer, V. A., Laakkonen, P., and Turunen, J., "Gauss–Laguerre modes with different indices in prescribed diffraction orders of a diffractive phase element," Opt. Commun. **175**, 301 (2000).
[24] Leach, J., Padgett, M. J., Barnett, S. M., Franke-Arnold, S., and Courtial, J., "Measuring the orbital angular momentum of a single photon," Phys. Rev. Lett. **88**(25), 257901 (2002).
[25] Lavery, M., Dudley, A., Forbes, A., Courtial, J., and Padgett, M., "Robust interferometer for the routing of light beams carrying orbital angular momentum," New J. of Phys. **13**(9), 093014 (2011).
[26] Berkhout, G. C. G., Lavery, M. P. J., Courtial, J., Beijersbergen, M. W., and Padgett, M. J., "Efficient sorting of orbital angular momentum states of light," Phys. Rev. Lett. **105**(15), 153601 (2010).
[27] Lavery, M. P. J., Robertson, D. J., Berkhout, G. C. G., Love, G. D., Padgett, M. J., and Courtial, J., "Refractive elements for the measurement of the orbital angular momentum of a single photon," Opt. Express **20**(3), 2110 (2012).
[28] Litvin, I., Dudley, A., and Forbes, A., "Poynting vector and orbital angular momentum density of superpositions of Bessel beams," Opt. Express 19(18), 16760-16771 (2011).
[29] Dudley, A., Litvin, I., and Forbes, A., "Quantitative measurement of the orbital angular momentum density of light," App. Opt. 51(7), 823-833 (2012).
[30] Litvin, I., Dudley, A., Roux, F. S., and Forbes, A., "Azimuthal decomposition with digital holograms," Opt. Express 20(10), 10996-11004 (2012).
[31] Dudley, A., Mhlanga, T., Lavery, M., McDonald, A., Roux, F. S., Padgett, M., and Forbes, A., "Efficient sorting of Bessel beams," Opt. Express 21(1), 165-171 (2013).
[32] Lavery, M. P. J., Berkhout, G. C. G., Courtial, J., and Padgett, M. J., "Measurement of the light orbital angular momentum spectrum using an optical geometric transformation," J. Opt. **13**, 064006 (2011).
[33] Berkhout, G. C. G., Lavery, M. P. J., Beijersbergen M. W., and Padgett, M. J., "Measuring orbital angular momentum superpositions of light by mode transformation," Opt. Lett. **36**, 1863–1865 (2011).

[34] Bryngdahl, O., "Geometrical transformations in optics," J. Opt. Soc. Am. **64**(8), 1092–1099 (1974).
[35] Hossack, W., Darling, A., and Dahdour, A., "Coordinate transformations with multiple computer-generated optical elements," J. Mod. Opt. **34**, 1235–1250 (1987).
[36] Saito, Y., Komatsu, S., and Ohzu, H., "Scale and rotation invariant real-time optical correlator using computer generated hologram," Opt. Commun. **47**(1), 8–11 (1983).
[37] Rop, R., Dudley, A., Lopez-Mariscal, C., and Forbes, A., "Measuring the rotation rates of superpositions of higher-order Bessel beams," J. Mod. Opt. **59**(3), 259–267 (2012).